Equilibrium structure and radial oscillations of dark matter admixed neutron stars

S.-C. Leung, M.-C. Chu, and L.-M. Lin

Department of Physics and Institute of Theoretical Physics, The Chinese University of Hong Kong, Hong Kong, China
(Received 30 November 2011; published 25 May 2012)

In Phys. Rev. D **84**, 107301 (2011), we presented our results on using a general relativistic two-fluid formalism to study the hydrostatic equilibrium configuration of an admixture of degenerate dark matter and normal nuclear matter. In this work, we present more analysis to complement our previous findings. We study the radial oscillation modes of these compact stars in detail. We find that these stars in general have two classes of oscillation modes. For a given total mass of the star, the first class of modes is insensitive to the dark-matter particle mass. They also reduce properly to the oscillation modes of the corresponding ordinary neutron star, with the same total mass, when the mass fraction of dark matter tends to zero. On the other hand, the second class of modes is due mainly to the dark-matter fluid. In the small dark-matter mass fraction limit, these modes are characterized purely by the oscillations of dark matter, while the normal matter is essentially at rest. In the intermediate regime where the mass fractions of the two fluids are comparable, the normal matter oscillates with the dark matter due to their coupling through gravity. In contrast to the first class of modes, the frequencies of these dark-matter dominated modes depend sensitively on the mass of dark-matter particles.

I. INTRODUCTION

Dark matter (DM) has gained more support for its existence from observations [1], such as galactic rotation curves [2–4], stability of bars in spiral galaxies [5–7], cosmological structure formation [8], and gravitational lensing [9]. However, the properties of DM particles, including their mass and interactions, are still largely unknown. Recent data from the DAMA [10] and CoGeNT [11] experiments are consistent with detecting light DM particles with mass ~ 10 GeV, which are incompatible with the null results from CDMS [12] and XENON [13]. On the theoretical side, it has been suggested that isospin-violating DM may be the key to reconciling these experimental results [14,15].

Despite the uncertainties on DM properties, it is still interesting to ask how DM would affect stellar structure and whether one could in turn make use of stellar objects to put constraints on DM. The role of DM in the first generation stars as stellar seeds, together with the possibility of DM annihilation as the first phase in stellar evolution, are examined in [16–19]. The impacts of DM on the evolution and formation of main-sequence stars are also examined [20–22]. The accretion and accumulation of non-self-annihilating DM particles in the cores of planets in our solar system and some pulsars are proposed to cause changes in their orbits [23–25]. Similarly, the effects of low-mass (~ 5 GeV) asymmetric DM particles on the solar composition, oscillations, and neutrino fluxes have been considered recently [26–28].

Besides main-sequence stars, one may infer DM particle properties through their effects on compact stars [29,30]. The effects of DM annihilation on the cooling curves of compact stars are also studied in [31–33]. The response of neutron stars (NS) under non-self-annihilating DM models, such as asymmetric matter [34] and mirror matter [35], have recently been studied. Neutron stars with DM cores are inherently two-fluid systems where the normal matter (NM) and DM couple essentially only through gravity. The technique used in recent studies of the structure of these dark-matter admixed neutron stars (DANS) is based on an *ad hoc* separation of the Tolman-Oppenheimer-Volkoff equation into two different sets for the normal and dark components inside the star [33,35,36]. This approach is motivated by the similarity of the structure equations between the relativistic and Newtonian ones, but it is not derived from first principle. In a previous paper [37], we made use of a general relativistic two-fluid formulation to study the equilibrium properties of DANS and proposed the existence of a new class of compact stars which are dominated by DM. These stars in general have a small NM core with radius of a few kilometer embedded in a ten-kilometer-sized DM halo. In the present work, we describe the formulation of two-fluid DANS in greater detail. We present additional analysis to study the equilibrium properties and the radial oscillation modes of these stars in detail.

The outline of this paper is as follows: In Sec. II we present the relevant equations used to study the static equilibrium structure, moment of inertia, and radial oscillation modes of DANS. In Sec. III we study the static equilibrium properties of DANS. Section IV discusses the stability of DANS and their radial oscillation modes in detail. Finally, we summarize our results in Sec. V. We use units where $G = c = 1$ unless otherwise noted.

II. TWO-FLUID FORMALISM FOR DANS

A. Static equilibrium models

The general relativistic two-fluid formalism was developed by Carter and his collaborators (see, e.g., [38]). It has been employed in the study of superfluid neutron stars (e.g., [39–42]), where the two fluids are normal and superfluid nuclear matter. In this work, we adopt the formulation in [39] to study DANS. Here we shall briefly summarize the equations we used and refer the reader to [39] for more details. To find the structure of a relativistic two-fluid star, one needs Einstein's equations $G_{\mu\nu} = 8\pi T_{\mu\nu}$ coupled with a matter source. In the two-fluid formulation, the matter source is governed by the master function $\Lambda(n^2, p^2, x^2)$, which is formed by the scalars $n^2 = -n_\alpha n^\alpha$, $p^2 = -p_\alpha p^\alpha$, and $x^2 = -n_\alpha p^\alpha$. The four vectors n^α and p^α are the conserved NM and DM number density currents, respectively.[1] The master function is a two-fluid analog of the equation of state (EOS) and $-\Lambda$ is taken to be the thermodynamics energy density.

For a static and spherically symmetric spacetime $ds^2 = -e^{\nu(r)}dt^2 + e^{\lambda(r)}dr^2 + r^2(d\theta^2 + \sin^2\theta d\phi^2)$, the Einstein equations and the fluid equations of motion reduce to the following differential equations:

$$\lambda' = \frac{1 - e^\lambda}{r} - 8\pi re^\lambda \Lambda(n, p), \qquad (1)$$

$$\nu' = -\frac{1 - e^\lambda}{r} + 8\pi re^\lambda \Psi(n, p), \qquad (2)$$

$$A_0^0 p' + B_0^0 n' + \tfrac{1}{2}(Bn + Ap)\nu' = 0, \qquad (3)$$

$$C_0^0 p' + A_0^0 n' + \tfrac{1}{2}(An + Cp)\nu' = 0, \qquad (4)$$

where the primes refer to derivative with respect to r and

$$A = -\frac{\partial\Lambda}{\partial x^2}, \qquad B = -2\frac{\partial\Lambda}{\partial n^2}, \qquad C = -2\frac{\partial\Lambda}{\partial p^2}. \quad (5)$$

The coefficients A_0^0, B_0^0, and C_0^0 are given by

$$A_0^0 = A + 2\frac{\partial B}{\partial p^2}np + 2\frac{\partial A}{\partial n^2}n^2 + 2\frac{\partial A}{\partial p^2}p^2 + \frac{\partial A}{\partial x^2}pn, \qquad (6)$$

$$B_0^0 = B + 2\frac{\partial B}{\partial n^2}n^2 + 4\frac{\partial A}{\partial n^2}np + \frac{\partial A}{\partial x^2}p^2, \qquad (7)$$

$$C_0^0 = C + 2\frac{\partial C}{\partial p^2}p^2 + 4\frac{\partial A}{\partial p^2}np + \frac{\partial A}{\partial x^2}n^2. \qquad (8)$$

---

[1]In the original work for superfluid neutron stars [39], n^α stands for the superfluid neutron number density currents, while p^α is the number density current for a conglomerate of all other charged constituents.

The generalized pressure Ψ in Eq. (2) is computed by

$$\Psi(n, p) = \Lambda + \mu n + \chi p, \qquad (9)$$

where $\mu = Bn + Ap$ and $\chi = Cp + An$.

Using Eqs. (1)–(4), one may calculate numerically the structure of a star by choosing suitable boundary conditions, namely, the central densities of the two fluids n_c and p_c, $\lambda(0) = \lambda'(0) = 0$ and $\nu'(0) = 0$. $\nu(0)$ is fixed by matching the solution with the Schwarzschild metric at the star surface $r = R$. The surface of the NM at $r = R_{\rm NM}$ is defined by the condition $n(R_{\rm NM}) = 0$. Similarly, we have the condition $p(R_{\rm DM}) = 0$ to define the surface of the DM fluid at $r = R_{\rm DM}$. In practice we choose n or $p = 10^{-5}$ fm^{-3} to define the surface of either fluid. It should be noted that, in general, the two surfaces are different (i.e., $R_{\rm NM} \neq R_{\rm DM}$). The star surface $r = R$, where a matching to the Schwarzschild metric is performed, is defined to be the larger one of $R_{\rm NM}$ and $R_{\rm DM}$. The total mass of the star is computed by

$$M = -4\pi \int_0^R dr r^2 \Lambda(r), \qquad (10)$$

while the total particle masses (baryonic masses) of NM and DM are computed by

$$M_{\rm NM} = 4\pi m_n \int_0^{R_{\rm NM}} dr r^2 e^{\lambda/2} n, \qquad (11)$$

$$M_{\rm DM} = 4\pi m_{\rm DM} \int_0^{R_{\rm DM}} dr r^2 e^{\lambda/2} p, \qquad (12)$$

where m_n and $m_{\rm DM}$ are the particle masses of NM and DM, respectively. It should be noted that the sum of the baryonic masses $M_{\rm NM} + M_{\rm DM}$ is in general different from the total mass M, which also includes the contributions from gravitational and internal energies.

B. Choice of EOS

In the two-fluid formalism, the master function Λ plays the role of the EOS information needed in the structure calculation. In this work, we assume that DM couples with NM only through gravity. Hence, the master function does not depend on the scalar product $x^2 = -n_\alpha p^\alpha$ and is separable in the sense that

$$\Lambda(n, p) = \Lambda_{\rm NM}(n) + \Lambda_{\rm DM}(p), \qquad (13)$$

$\Lambda_{\rm NM}(n)$ and $\Lambda_{\rm DM}(p)$ being the negative of energy densities of NM and DM at a given number density, respectively. These assumptions imply that the coefficients $A = A_0^0 = 0$ in our study.

We choose the Akmal-Pandharipande-Ravenhall (APR) EOS [43] for NM [and Baldo-Bombaci-Burgio (BBB)2 EOS [44] as well for comparison] and ideal degenerate Fermi gas EOS for DM. As discussed earlier, DM candidates in the mass range of a few GeV are of great interest

recently. We shall thus consider fermionic DM particles in this mass range.

C. Moment of inertia

Besides global quantities like gravitational mass and radius, it is also interesting to study the moment of inertia of DANS since it is measurable and plays an important role in the physics of ordinary neutron stars.

The moment of inertia of a rotating star in general relativity is defined by $I = J/\Omega$ in the slow rotation limit, where J and Ω are, respectively, the angular momentum and angular velocity. Here we follow the formulation developed in [40] to calculate the angular momentum of a two-fluid star in the slow rotation limit. First, we need to compute the frame dragging of the star due to its rotation. In general, DM and NM can rotate with different velocities, Ω_p and Ω_n, respectively. The frame dragging ω is given by [40]

$$\frac{1}{r^4}(r^4 e^{-(\lambda+\nu)/2}L_n')' - 16\pi e^{(\lambda-\nu)/2}(\Psi_0 - \Lambda_0)L_n$$
$$= 16\pi e^{(\lambda-\nu)/2}\chi_0 p_0(\Omega_n - \Omega_p), \qquad (14)$$

where

$$L_n = \omega - \Omega_n, \qquad (15)$$

$$L_p = \omega - \Omega_p. \qquad (16)$$

It should be noted that Eq. (14) is formally identical to the equation obtained by Hartle [45] for one-fluid stars except for the nonzero source term on the right-hand side. In particular, the corotating case ($\Omega_n = \Omega_p$) reduces to the one-fluid result. To integrate this equation with higher accuracy, one defines a new variable

$$T_n = (r^4 e^{-(\lambda+\nu)/2}L_n'). \qquad (17)$$

We can decompose Eq. (14) into two first-order equations:

$$T_n' = 16\pi r^4 e^{(\lambda-\nu)/2}(\Psi_0 - \Lambda_0)L_n$$
$$+ 16\pi r^4 e^{(\lambda-\nu)/2}\chi_0 p_0(\Omega_n - \Omega_p), \qquad (18)$$

$$L_n' = \frac{1}{r^4}e^{(\lambda+\nu)/2}S_n. \qquad (19)$$

We integrate the two variables T_n and L_n from the origin to the surface subject to the boundary condition,

$$L_n(R) = -\Omega_n - \frac{R}{3}\left(\frac{dL_n}{dr}\right)_{r=R}. \qquad (20)$$

With L_n and L_p calculated above, the total angular momentum of the star is given by

$$J = -\frac{8\pi}{3}\int_0^R dr r^4 e^{(\lambda-\nu)/2}(\mu_0 n_0 L_n + \chi_0 p_0 L_p). \qquad (21)$$

When the master function Λ is independent of the scalar product $x^2 = -n_\alpha p^\alpha$ (as we assume in this work), the two terms in the integral correspond to the NM and DM angular momenta (J_n and J_p), respectively [40]. We can thus define the moments of inertia $I_n = J_n/\Omega_n$ and $I_p = J_p/\Omega_p$. I_n and I_p depend on the nonrotating background quantities of NM and DM separately. The total moment of inertia of DANS is then defined by $I = I_n + I_p$.

D. Equations for radial oscillations

To study the stability and radial oscillation modes of DANS, we use the set of equations for radial perturbations of a two-fluid star derived in Sec. IV B of [39]. We shall discuss our numerical scheme in solving the eigenvalue problem in detail.

Assuming DM has no interaction with NM except through gravity (in the sense that the coefficient $A = A_0^0 = 0$), and adopting the notation $S_n = rnW_n$ and $S_p = rpW_p$, the set of equations governing radial oscillations is simplified to

$$\frac{\omega^2}{r^2}e^{(\lambda-\nu)/2}(BS_n) = \left(-\frac{e^{(\nu-\lambda)/2}}{r^2}[B_0^0 S_n'] + \frac{1}{2}\frac{e^{\nu/2}}{r}[B_0^0 n]\right.$$
$$\left. \times [8\pi e^{\lambda/2}(\chi S_p + \mu S_n)]\right)' + \frac{1}{2}\mu H_0', \qquad (22)$$

$$\frac{\omega^2}{r^2}e^{(\lambda-\nu)/2}(CS_p) = \left(-\frac{e^{(\nu-\lambda)/2}}{r^2}[C_0^0 S_p'] + \frac{1}{2}\frac{e^{\nu/2}}{r}[C_0^0 p]\right.$$
$$\left. \times [8\pi e^{\lambda/2}(\chi S_p + \mu S_n)]\right)' + \frac{1}{2}\chi H_0', \qquad (23)$$

where

$$H_0' = 4\pi r e^{\nu/2+\lambda}\left(p^2 C_0^0 + n^2 B_0^0 - 2\Psi - \frac{1}{4\pi r^2}\right)H_2$$
$$- \frac{8\pi e^{(\nu+\lambda)/2}}{r}(pC_0^0 S_p' + nB_0^0 S_n'), \qquad (24)$$

$$H_2 = \frac{8\pi e^{\lambda/2}}{r}(\chi S_p + \mu S_n). \qquad (25)$$

Note that the quantities W_n and W_p are related to the radial component of the Lagrangian displacement of both fluids by $\delta\xi_n^r = e^{-\lambda/2}W_n e^{i\omega t}/r$ and $\delta\xi_p^r = e^{-\lambda/2}W_p e^{i\omega t}/r$.

The radial oscillation modes can be solved by specifying the boundary conditions at the core, and the correct eigenvalues can be obtained by checking whether the boundary conditions at the surfaces of both fluids are satisfied. In this problem, we have 4 degrees of freedom at the core, namely $S_n(0)$, $S_p(0)$, $S_n'(0)$, and $S_p'(0)$. Note that the four variables cannot be set arbitrarily, otherwise the boundary conditions of both fluids at the surfaces cannot be satisfied simultaneously.

The boundary condition at the surface of each fluid is given by the vanishing of the Lagrangian density variation of the fluid. The Lagrangian density variations are given by [39]

$$\frac{\Delta n}{n} = e^{-\lambda/2}\left(\frac{W_n}{r^2} + \frac{W_n'}{r}\right) - \frac{1}{2}H_2, \qquad (26)$$

$$\frac{\Delta p}{p} = e^{-\lambda/2}\left(\frac{W_p}{r^2} + \frac{W_p'}{r}\right) - \frac{1}{2}H_2. \qquad (27)$$

Hence, we require the boundary conditions $\Delta n/n = 0$ at $r = R_{NM}$ and $\Delta p/p = 0$ at $r = R_{DM}$.

To find the correct boundary conditions at the core, we first choose S_n to be unity. $S_n'(0)$ is chosen according to the Taylor expansion of $S_n(r)$ and the regularity condition of S_n near the center. Namely, we have

$$S_n(r) = S_n(0)r^3 + O(r^5), \qquad (28)$$

from which we have $S_n'(0) = 3S_n(0)$ [similarly, we have $S_p'(0) = 3S_p(0)$]. $S_p(0)$ is chosen such that the boundary condition of the inner surface of a DANS model can be satisfied. In practice, we first choose a trial eigenvalue ω and a trial $S_p(0)$ (without loss of generality, we assume $R_{DM} < R_{NM}$ in this discussion). Then, we integrate up to the inner surface of the DANS model. If the boundary condition at the inner surface is not satisfied, a new trial of $S_p(0)$ is used and the integration is repeated. Once a correct trial of $S_p(0)$ is found to satisfy the boundary condition at the inner surface, we continue the integration up to the outer surface and check whether the boundary condition at the outer surface is satisfied. We obtain the eigenvalue if the trial ω can satisfy the boundary condition of the outer surface.

III. STATIC EQUILIBRIUM PROPERTIES OF DANS

A. General properties of DANS

In Fig. 1(a), we show the mass-radius relations of DANS for different DM mass fractions defined by

$$\epsilon = \frac{M_{DM}}{M_{NM} + M_{DM}}. \qquad (29)$$

The NM is modeled by the APR EOS and the DM particle mass is $m_{DM} = 1$ GeV.

The case $\epsilon = 0$ corresponds to ordinary NS without DM. For increasing ϵ, representing DANS with higher DM proportion, we observe two results: first, the maximum stable mass decreases and the stars also have smaller radii. For example, for $\epsilon = 0.2$, the mass and radius of the maximum stable mass configuration are decreased by 35% and 9% respectively, compared to the case with $\epsilon = 0$. Second, the M-R curve flattens as ϵ increases, such as the one shown for $\epsilon = 0.8$. For intermediate DM mass fraction, such as $\epsilon = 0.4$, the curves are made of two

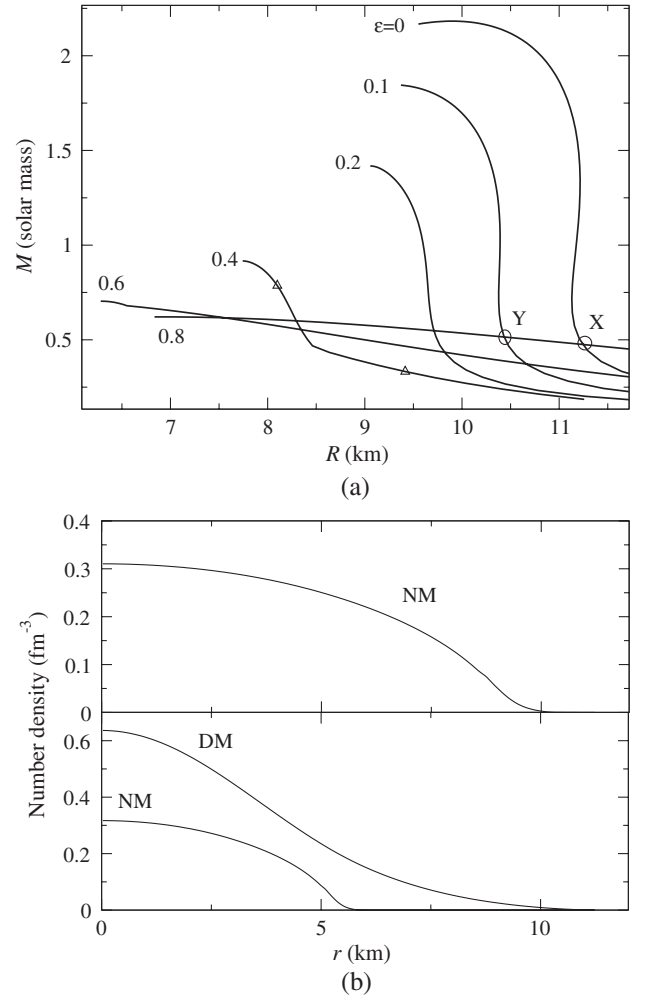
FIG. 1. Upper plot (a): Mass-radius relations of DANS for different DM mass fraction ϵ. The NM is modeled by the APR EOS and the DM particle mass is 1 GeV. Masses are in unit of $M_\odot$. Lower plot (b): Density profiles of the star models at the point X in Fig. 1(a) for an ordinary NS ($\epsilon = 0$, upper panel) and a DM dominated star ($\epsilon = 0.8$, lower panel). Both star models have mass $0.475M_\odot$ and $R = 11.25$ km. For the DM dominated star (lower panel), $M_{NM} = 0.0981M_\odot$, $M_{DM} = 0.3923M_\odot$, and $R_{NM} = 6.29$ km.

parts: The curve is flat at large R, but at small R, it is qualitatively similar to the curve for ordinary NS. The above patterns suggest that a new class of compact stars exists, when ϵ is sufficiently large. We will show that these DM dominated stars are qualitatively different from ordinary NS in many aspects.

We plot in Fig. 1(b) the density profiles of the DANS models marked as point X in Fig. 1(a). The upper panel is for the case $\epsilon = 0$ while the lower one is for the case $\epsilon = 0.8$. Although both models have the same total mass and radius, the mass in the upper one is contributed only by NM, while the mass in the lower one is mainly contributed by DM. For the case $\epsilon = 0.8$, it is seen that a small NM core is embedded in a larger DM halo.
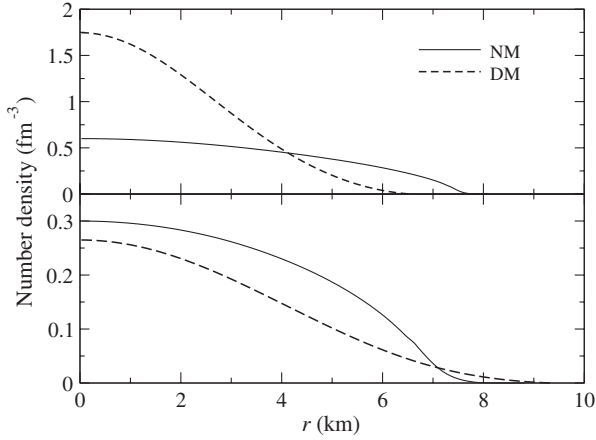
FIG. 2. Density profiles for two star models with $\epsilon = 0.4$ with the APR EOS for NM and ideal degenerate gas EOS for DM with DM particle mass = 1 GeV. The solid (dashed) lines are for NM (DM). Upper plot: $M = 0.780 M_\odot$, $R = 8.10$ km, $R_{DM} = 6.60$ km. Lower plot: $M = 0.332 M_\odot$, $R = 9.42$ km, $R_{NM} = 8.84$ km.

Next we plot in Fig. 2 two distinctive models for the case $\epsilon = 0.4$ [marked with triangles in Fig. 1(a)]. One star is chosen from the part of the M-R curve which is similar to that of ordinary NS, while another star is chosen from the other side. We choose one model (upper panel in Fig. 2) to have $M = 0.780 M_\odot$, $R = 8.10$ km, $R_{DM} = 6.60$ km and the other (lower panel) to have $M = 0.332 M_\odot$, $R = 9.42$ km, $R_{NM} = 8.84$ km. For the former model (upper panel), we see that the DM is engulfed by NM. However, the situation is reversed for the latter model (lower panel).

The scaled moment of inertia $\tilde{I} \equiv I/MR^2$ of DANS is plotted as a function of the compactness (M/R, in the unit solar mass/km) in Fig. 3. In [46], Bejger and Haensel found an approximate universal relation between $\tilde{I}$ and compactness ($z \equiv (M/M_\odot)/(\text{km}/R)$):

$$\tilde{I} = \frac{z}{0.1 + 2z}, \qquad z < 0.1, \tag{30}$$

$$\tilde{I} = \frac{2}{9}(1 + 5z), \qquad z > 0.1. \tag{31}$$

This formula is shown as the dashed line in Fig. 3. The vertical lines (with arrows) at $z = 0.05$, 0.1, and 0.15 represent the range of values of $\tilde{I}$ obtained by a large set of EOS models which were used to obtain the formula. They can be regarded as the error bars of Eqs. (30) and (31) at those values of M/R. The circles in the figure correspond to an ordinary neutron star ($\epsilon = 0$) and DM dominated star ($\epsilon = 0.8$) at the point X in Fig. 1(a). While the scaled moment of inertia of ordinary neutron stars can be modeled approximately by Eqs. (30) and (31), Fig. 3 shows that $\tilde{I}$ of DANS depends sensitively on the amount of DM. In particular, for the DM dominated sequence $\epsilon = 0.8$, the value of $\tilde{I}$ is significantly smaller than that allowed for ordinary neutron stars with the same compactness.
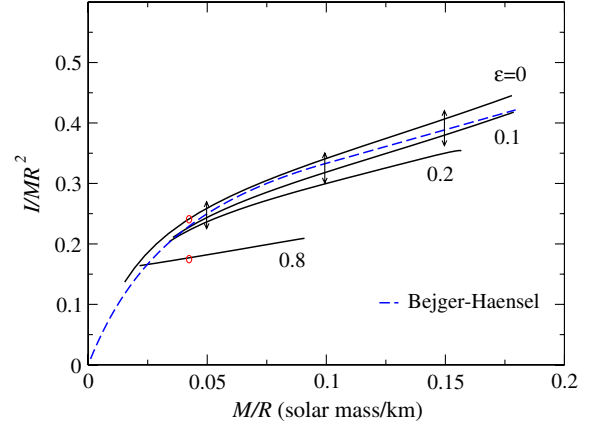

FIG. 3 (color online). I/MR^2 of DANS against M/R with the APR EOS for NM and ideal degenerate Fermi gas EOS for DM, with DM particle mass of 1 GeV. The dashed line corresponds to the numerical fitting found by Bejger and Haensel [46]. The circles correspond to the two stellar models ($\epsilon = 0$ and 0.8) at the point X in Fig. 1(a)

B. Linear response of DANS

Here we study the effects of DM in the core on the structure of DANS at the small M_{DM} limit. In the linear regime, namely a DANS with small M_{DM}, the radius and moment of inertia of the star vary linearly with M_{DM}. But the slope of the linear variation depends on the stiffness of the NM EOS. The stiffer the NM EOS is, the smaller the contraction results.

In Fig. 4(a) we plot R/R_0 against M_{DM}, where R_0 is the radius without DM (i.e., an ordinary NS), for $M_{NM} = 1.4$, 1.6, and $1.8 M_\odot$. We see that the relative changes in radii are linear in M_{DM}. For a fitting in the form

$$\frac{R}{R_0} = 1 + a_1 M_{DM}, \tag{32}$$

we find that $a_1 \approx -0.5$ for the APR EOS and $a_1 \approx -0.7$ for the BBB2 EOS. The larger magnitude of a_1 for BBB2 EOS is due to the fact that this EOS is softer than the APR EOS. We also see that a_1 is essentially independent of M_{NM}. The effect from DM is no longer linear for large M_{DM}.

In Fig. 4(b) we plot I/I_0 against M_{DM}, where I_0 is the moment of inertia of a NS without DM, for three different values of M_{NM} as above. The change in I is almost the same for the three cases:

$$\frac{I}{I_0} = 1 + a_2 M_{DM}, \tag{33}$$

with $a_2 \approx -0.6$ for the APR EOS and $a_2 \approx -0.9$ for the BBB2 EOS. Again, the value of a_2 does not depend strongly on M_{NM}.

(a)

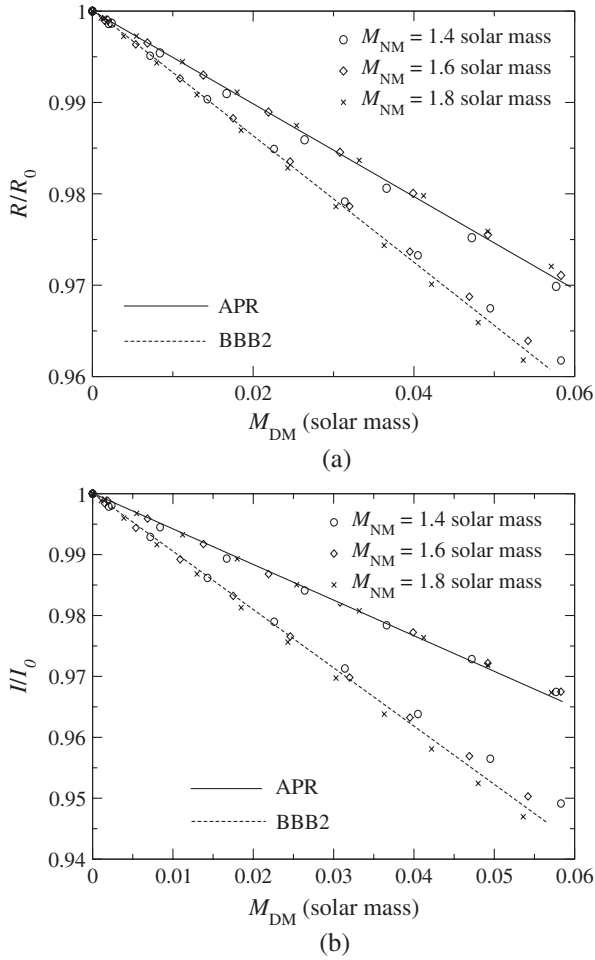(b)

FIG. 4. Upper plot (a): R/R_0 is plotted against M_{DM} (in $M_\odot$) for the APR and BBB2 EOS for NM and ideal degenerate Fermi gas EOS for DM, with DM particle mass of GeV. R_0 is the NS radius without DM. Lower plot (b): I/I_0 against M_{DM} (in $M_\odot$). I_0 is the moment of inertia without DM.

C. Effects of DM particle mass

As discussed in Sec. I, DM candidates in the mass range a few GeV is of great interest recently. We shall thus study the effects of DM particle mass m_{DM} in this range. We shall compare the equilibrium properties of DANS with different m_{DM}. In this part, we use the APR EOS to model the NM.

First, we plot in Fig. 5(a) the total mass M against the minimum radius R_{min} of stable stars allowed for a given m_{DM}. We present the results for three different cases $m_{DM} = 1$, 4, and 7 GeV. We also plot the M-R curve (solid line) for ordinary NS without DM for comparison. For fixed M and m_{DM}, the radius of the star decreases as the mass fraction of DM increases (i.e., the star becomes more compact). We define R_{min} to be the minimum radius below which the star becomes unstable. For example, Fig. 5(a) shows that the minimum radius allowed for a DANS with total mass $M = 1M_\odot$ and DM particle mass
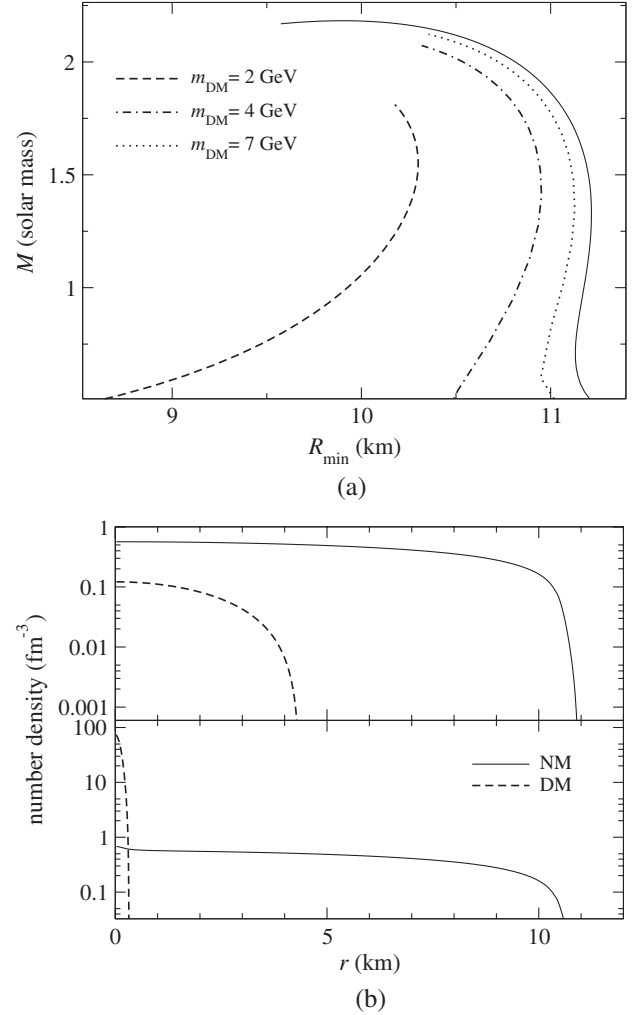

(a)

(b)

FIG. 5. Upper plot (a): Total mass M is plotted against the minimum radius R_{min} of stable stars allowed for a given DM particle mass m_{DM}. The solid line is the M-R curve for ordinary NS without DM for comparison. Lower plot (b): Number density profiles of NM (solid lines) and DM (dashed lines) for two stars with the same $M = 1.4M_\odot$ and $M_{DM} = 0.01M_\odot$, but with $m_{DM} = 1$ GeV (upper panel) and 7 GeV (lower panel).

$m_{DM} = 2$ GeV is about 10 km. We also see that R_{min} increases with m_{DM} for a given M.

In Fig. 5(b), we plot the density profiles of two stars with the same $M = 1.4M_\odot$ and $M_{DM} = 0.01M_\odot$, but with different DM particle mass $m_{DM} = 1$ GeV (upper panel) and 7 GeV (lower panel). In Fig. 5(b), we see that with a higher DM particle mass $m_{DM} = 7$ GeV, the DM core shrinks to a very small size of about 0.3 km, compared to 4.3 km for the case $m_{DM} = 1$ GeV. Also, the density of the DM core is much higher than that of the NM for $m_{DM} = 7$ GeV.

Finally, in Fig. 6 we plot the maximum stable mass for DANS models with $\epsilon = 0.1$ but with m_{DM} ranging from 1 to 5 GeV. The maximum stable mass decreases with m_{DM}. The reason is as follows: the NM and DM are assumed to be noninteracting (except through gravity), and the DM
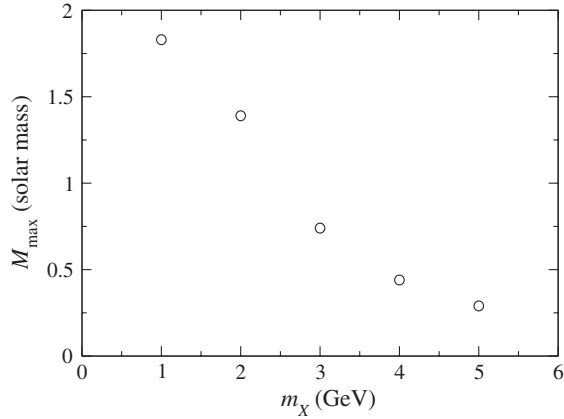
FIG. 6.   Maximum stable mass M_{max} is plotted against the DM particle mass m_X for a fixed amount of DM specified by $\epsilon = 0.1$.

core is supported only by its own degenerate pressure. It is well known that the maximum mass limit for a self-gravitating Fermi gas decreases as the particle mass increases. Hence, the onset of the collapse of a degenerate DM core is responsible for the dependence of M_{max} on m_{DM} as seen in Fig. 6. Furthermore, the allowed mass fraction of DM inside a stable DANS decreases significantly as m_{DM} increases. For example, stable DANS models with $M_{\mathrm{DM}} \approx 0.1 M_{\odot}$ can only be formed by DM particles of mass less than about 3 GeV.

IV. RADIAL OSCILLATIONS OF DANS

In this section we study the radial oscillation eigenfrequencies and eigenfunctions of DANS. We show that all DANS with central energy density less than that of the maximum mass configuration, regardless of the mass fraction ϵ of DM, are stable. We also study the effect of ϵ and DM particle mass m_{DM} on the radial oscillation modes. In this section, we use the APR EOS to model the NM. Unless otherwise noted, the DM particle mass m_{DM} is chosen to be 1 GeV.

A. One-fluid limit

We first present some tests to check the validity of the numerical code. We calculate the oscillation modes of ordinary NS modeled by the APR EOS in the one-fluid limit using our two-fluid code. In practice, this is achieved by setting the central density of DM to a sufficiently small number so that the star is essentially composed of NM only. In Fig. 7(a) we plot the total mass (upper panel) and fundamental mode frequency squared (lower panel) against the central energy density. We set the central number density of DM to be 8 orders of magnitude smaller than that of NM in the calculations. As expected from the study of ordinary NS, Fig. 7(a) shows that the fundamental mode frequency passes through zero at the central energy density corresponding to the maximum mass configuration. The point $\omega^2 = 0$ marks the onset of instability.
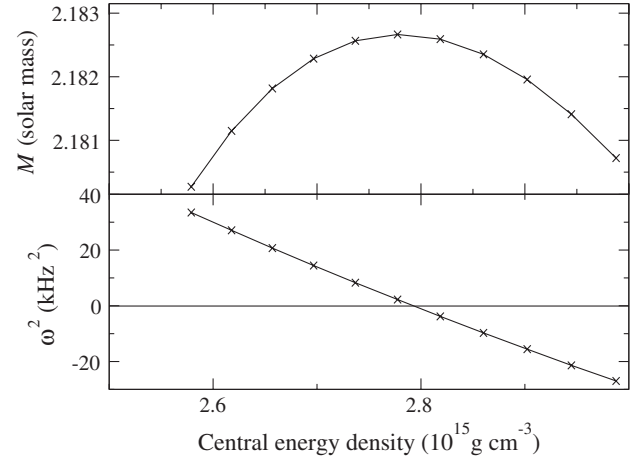
(a)
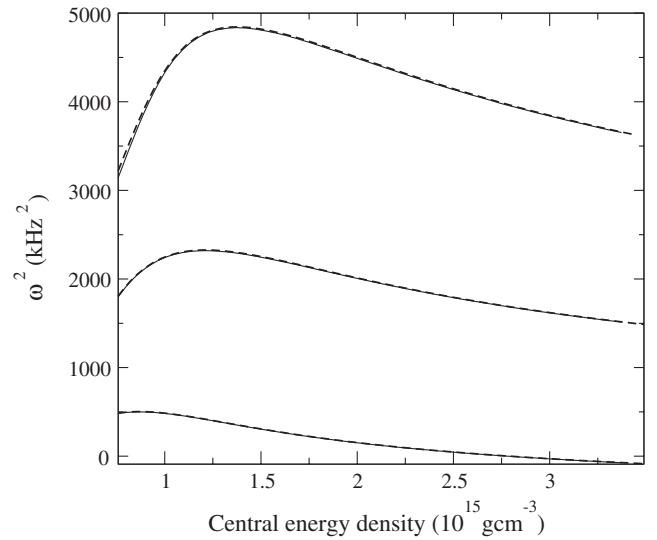
(b)

FIG. 7.   Upper plot (a): Total mass (upper panel) and fundamental mode frequency squared (lower panel) are plotted against the central energy density for ordinary NS modeled by the APR EOS. Lower plot (b): Frequency squared for the first three modes are plotted against the central energy density for ordinary NS modeled by the APR EOS. The dashed lines are obtained by the two-fluid code in the one-fluid limit. The solid lines are obtained by a one-fluid code (see text).

Beyond this critical density, the stars are unstable against radial perturbations.

We compare in Fig. 7(b) the frequencies of the first three modes calculated separately by the two-fluid code (dashed lines) and a different code (solid lines) based on the standard one-fluid formulation [47]. We see that the two sets of mode frequencies agree very well.

B. Oscillation modes of DANS

In Fig. 8(a), we plot the total mass (upper panel) and the fundamental mode frequency squared (lower panel) against the central energy density for $\epsilon = 0.2$. Similar to
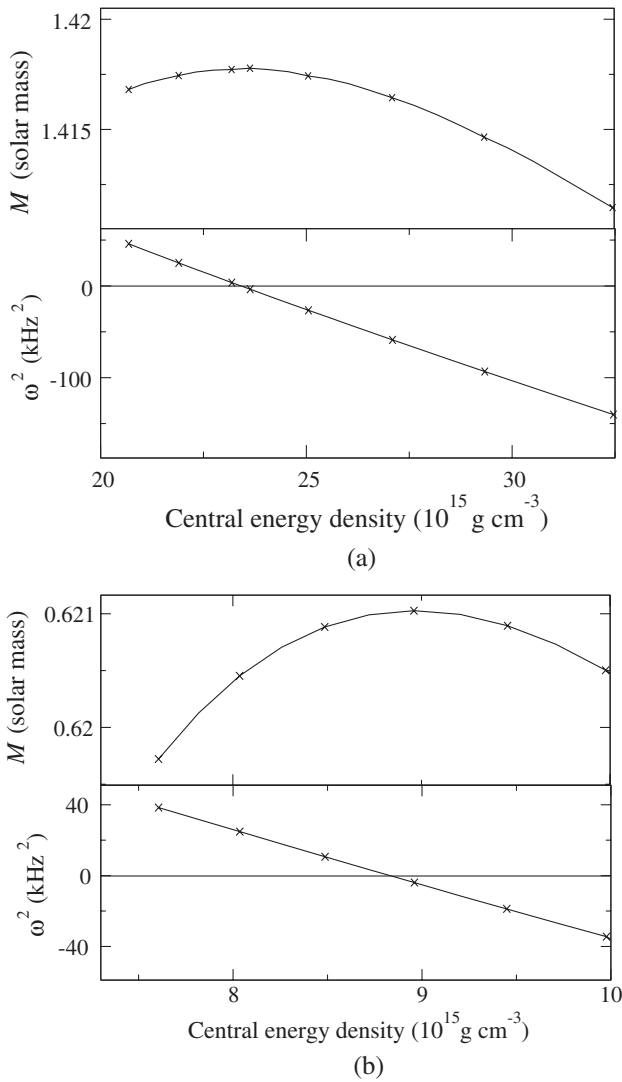
FIG. 8. Upper plot (a): Total mass and fundamental mode frequency squared are plotted against the central energy density for $\epsilon = 0.2$. Lower plot (b): Same as Fig. 8(a), but for $\epsilon = 0.8$.

FIG. 9. Upper plot (a): The frequency squared for the first four oscillation modes are plotted against ϵ. The total mass $M = 1.4M_\odot$ is fixed. The circles indicate the absence of the corresponding modes at the limit $\epsilon = 0$. Lower plot (b): The Lagrangian density variations of the first four modes of a DANS with $\epsilon = 0.005$ and total mass $M = 1.4M_\odot$.

the ordinary NS (one-fluid) case, the mode frequency passes through zero at the central energy density corresponding to the maximum mass configuration. The stars are unstable beyond this critical density. For DANS with central density lower than the critical density, they are stable against radial perturbations. In Fig. 8(b) we show the case $\epsilon = 0.8$ for the DM dominated sequence. Our results confirm the stability of DANS. In particular, the new class of DM dominated compact stars with a NM core embedded in a ten-kilometer sized DM halo are shown to be stable.

In Fig. 9(a) we plot the first four mode frequency squared of DANS as a function of ϵ. The total mass $M = 1.4M_\odot$ is fixed. We can see from the frequency of the fundamental mode ($n = 1$) that increasing ϵ (i.e., the mass fraction of DM) has the effect of decreasing the stability of the star. The fundamental mode frequency
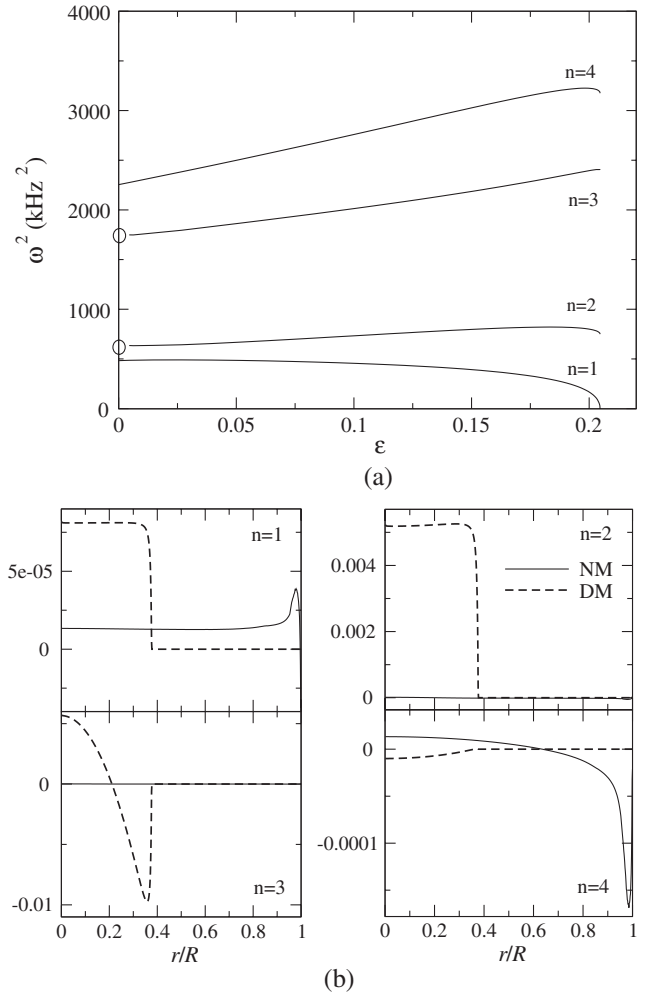
drops sharply to zero for ϵ slightly above 0.2, hence indicating the onset of instability. We also see that the frequencies of the higher order modes ($n = 2, 3, 4$) in general increase with ϵ. It is interesting to notice that the second ($n = 2$) and third ($n = 3$) modes are missing in the one-fluid limit when $\epsilon = 0$. In Fig. 9(b), we show the Lagrangian variations of NM [Eq. (26)] and DM [Eq. (27)] for the first four modes of a star with $\epsilon = 0.005$. The solid (dashed) lines are the profiles of NM (DM). Note that the DM core extends to about $0.4R$, where R is the radius of the star.

First, let us consider the $n = 1$ and $n = 4$ modes. They have proper limits at $\epsilon = 0$. For the fundamental mode ($n = 1$), in the DM core where the two fluids coexist, the density variations of NM and DM are in phase. For the $n = 4$ mode, the density variation of NM (DM) is larger (smaller) than zero in the DM core. Hence, the
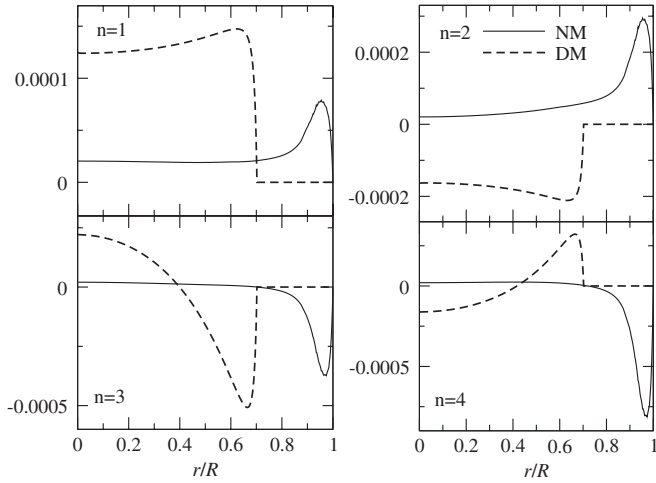
FIG. 10.   The Lagrangian density variations of the first four modes for the ordinary DANS with $\epsilon = 0.1$ at the point Y in Fig. 1(a).
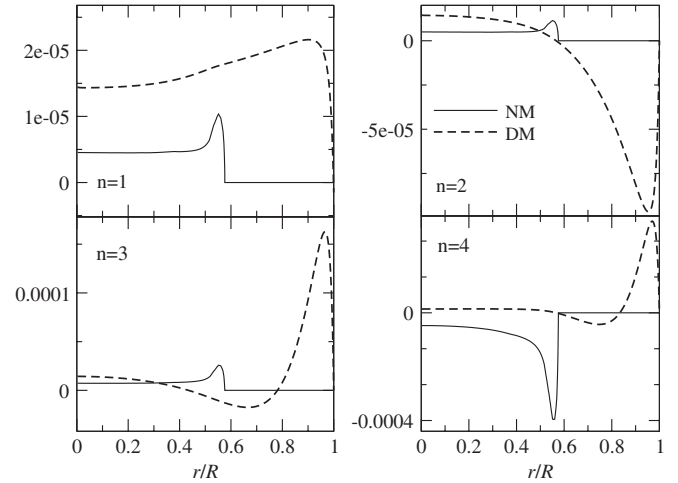

FIG. 11.   The Lagrangian density variations of the first four modes for the DM dominated compact star with $\epsilon = 0.8$ at the point Y in Fig. 1(a).

two fluids are countermoving in this case. On the other hand, for the $n = 2$ and $n = 3$ modes, we see that the density variation of NM is much smaller than that of DM. These modes are dominated by DM motion in the DM core. They do not exist when there is no DM (i.e., $\epsilon = 0$). However, they emerge even for a very small mass fraction of DM.

To further study the oscillation modes of DANS, we choose the two stellar models at the point Y in Fig. 1(a). The stars have the same mass $M = 0.541 M_\odot$ and radius $R = 9.68$ km, but with different mass fraction of DM. The model with $\epsilon = 0.1$ is an ordinary DANS. The model with $\epsilon = 0.8$ is a DM dominated compact star with a small NM core embedded in a ten-kilometer sized DM halo. The Lagrangian variations of the first four oscillation modes for the model with $\epsilon = 0.1$ are plotted in Fig. 10. For the $n = 1$ and $n = 4$ modes, the general patterns of the modes are qualitatively the same as the case $\epsilon = 0.005$ in Fig. 9(b). The two fluids are in large part comoving (countermoving) for the $n = 1$ ($n = 4$) mode. For the $n = 2$ and $n = 3$ modes, which are dominated by DM motion in the case $\epsilon = 0.005$, we now see that there are significant density variations of NM near the stellar surface. This can be understood by the fact that the two fluids are coupled through gravity. For a very small ϵ, the motion of a small amount of DM basically has no effect on the NM. Hence, the NM essentially decouples from the DM and does not move in the $n = 2$ and $n = 3$ DM dominated modes. However, when the mass fraction of DM is comparable to NM, the coupling between the two fluids becomes stronger and, hence, we can see a large density variation of NM.

The Lagrangian variations of the first four oscillation modes for the DM dominated model with $\epsilon = 0.8$ are plotted in Fig. 11. We see that for the "ordinary" $n = 1$ and $n = 4$ modes the maximum density variations of the

two fluids near their surfaces are comparable. Note that the surface of the NM core is at about $0.6R$, where the radius of the star R is defined by the radius of the DM halo in this model. However, for the $n = 2$ and $n = 3$ DM dominated modes, the maximum density variation of DM is much larger than that of NM.

C. Effects of DM particle mass

To end this section, we study the effects of DM particle mass on the mode frequencies. In Fig. 12 we show the frequencies of the first five modes of a DANS with $M = 1.4 M_\odot$ and $M_{DM} = 0.01 M_\odot$ as a function of DM particle mass m_{DM}. For $m_{DM} = 1$ GeV, the second and third modes correspond to the $n = 2$ and $n = 3$ DM dominated modes studied above. We see that the frequencies of these
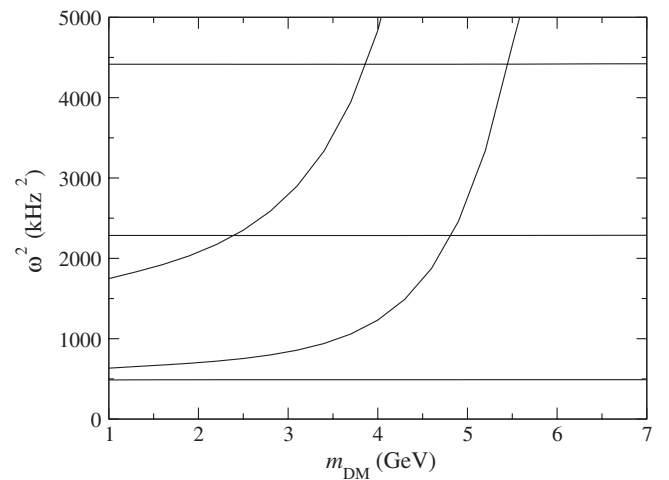

FIG. 12.   Frequency squared for the first five oscillation modes are plotted against the DM particle mass m_{DM}. The total mass $M = 1.4 M_\odot$ and DM core mass $M_{DM} = 0.01 M_\odot$ of the stars are fixed.

modes increase with m_{DM}, while the other modes are essentially independent of m_{DM}. It is known that the radial oscillation mode frequency (squared) scales with the density of the star. Also, for a fixed DM core mass, the DM core becomes denser as m_{DM} increases [see Fig. 5(b)]. Hence, the frequencies of the DM dominated modes depend strongly on m_{DM}.

It is also interesting to notice that, while the second and third modes are DM dominated modes in the case $m_{DM} = 1$ GeV, this is in general not true for other m_{DM}. For example, in the case $m_{DM} = 3$ GeV, it is the second and fourth modes that are DM dominated modes. For $m_{DM} = 5$ GeV, the DM dominated mode first appears only in the third mode.

V. CONCLUSIONS

In this paper, we have studied the equilibrium properties and radial oscillation modes of DANS using a general relativistic two-fluid formalism. We model the NM by realistic nuclear matter EOS. The DM particles are assumed to be non-self-annihilating and described by an ideal degenerate Fermi gas. Our results suggest that the structure of these stars depends strongly on the DM fluid. In particular, we found a new class of compact stars which are dominated by DM. These stars in general have a small NM core with radius a few km embedded in a larger ten-kilometer-sized DM halo. Since only the NM core can emit thermal radiation, the detection of a compact star with a thermally radiating surface of such a small size could provide strong evidence for the existence of DANS. Furthermore, these DM dominated stars also have rather different mass-radius relations and scaled moment of inertia compared to ordinary NS without DM. We have also studied how the radius R and moment of inertia I of a star with fixed NM baryonic mass M_{NM} change as the DM core mass M_{DM} increases. In the small M_{DM} limit, we see that R and I decrease linearly as M_{DM} increases. The slopes of the linear variations depend essentially only on the NM EOS, but not on the value of M_{NM}.

We have performed a radial perturbation analysis and studied the oscillation modes of DANS in general. The stability of DANS is shown explicitly by calculating the frequency of the fundamental mode. For a sequence of stars with a fixed DM mass fraction, we see that the fundamental mode frequency passes through zero at the central energy density corresponding to the maximum mass configuration. Similar to the analysis of ordinary NS, this point marks the onset of instability.

Besides the fundamental mode, we have also studied the first few higher order oscillation modes. We see that DANS in general have two classes of oscillation modes. The first class of modes has proper limit when the DM mass fraction tends to zero, namely these modes reduce to the same set of modes for ordinary NS without DM. On the other hand, the second class of modes is due mainly to DM. In the limit of a small DM mass fraction, these modes are characterized purely by the oscillations of DM. The NM fluid is essentially at rest. In the intermediate case where the mass fractions of NM and DM are comparable, the NM fluid oscillates with the DM fluid due to their coupling through gravity. On the other hand, the amplitude of DM oscillations is much larger than that of NM in the case of DM dominated stars. We also see that the frequencies of these oscillation modes depend strongly on the DM particle mass.

Finally, it should be pointed out that the formation mechanism of DANS is not clear. However, our main focus in this work is to study the properties of these theoretical objects, if they exist. The formation process of these compact dark-matter compact objects cannot yet be modeled in current N-body simulations, which mainly focus on the structure formation in galactic or cosmological scales.

ACKNOWLEDGMENTS

[1] M. Roos, arXiv:1001.0316v2.
[2] Y. Sofue, M. Honma, and T. Omodaka, Publ. Astron. Soc. Jpn. **61**, 227 (2009).
[3] R. Catena and P. Ullio, J. Cosmol. Astropart. Phys. 08 (2010) 004.
[4] M. Weber and W. de Boer, Astron. Astrophys. **509**, A25 (2010).
[5] R. H. Miller, K. H. Prendergast, and W. J. Quirk, Astrophys. J. **161**, 903 (1970).
[6] F. Hohl, Astrophys. J. **168**, 343 (1971).
[7] J. P. Ostriker and P. J. E. Peebles, Astrophys. J. **186**, 467 (1973).
[8] V. Springel *et al.*, Nature (London) **435**, 629 (2005).
[9] R. Massey *et al.*, Nature (London) **445**, 286 (2007).
[10] R. Bernabei *et al.* (DAMA Collaboration), Eur. Phys. J. C **56**, 333 (2008).
[11] C. E. Aalseth *et al.* (CoGeNT Collaboration), Phys. Rev. Lett. **106**, 131301 (2011).
[12] Z. Ahmed *et al.* (CDMS Collaboration), Phys. Rev. Lett. **106**, 131302 (2011).
[13] E. Aprile *et al.* (XENON100 Collaboration), Phys. Rev. Lett. **105**, 131302 (2010).
[14] J. L. Feng, J. Kumarb, D. Marfatia, and D. Sanford, Phys. Lett. B **703**, 124 (2011).

[15] M. T. Frandsen, F. Kahlhoefer, J. March-Russell, C. McCabe, M. McCullough, and K. Schmidt-Hoberg, Phys. Rev. D **84**, 041301 (2011).

[16] D. Spolyar, K. Freese, and P. Gondolo, Phys. Rev. Lett. **100**, 051101 (2008).

[17] D. Spolyar, P. Bodenheimer, K. Freese, and P. Gondolo, Astrophys. J. **705**, 1031 (2009).

[18] E. Ripamonti, F. Iocco, A. Ferrara, R. Schneider, A. Bressan, and P. Marigo, Mon. Not. R. Astron. Soc. **406**, 2605 (2010).

[19] S. Hirano, H. Umeda, and N. Yoshida, Astrophys. J. **736**, 58 (2011).

[20] J. Casanellas and I. Lopes, Astrophys. J. **705**, 135 (2009).

[21] J. Casanellas and I. Lopes, Astrophys. J. **733**, L51 (2011).

[22] I. Lopes, J. Casanellas, and D. Eugenio, Phys. Rev. D **83**, 063521 (2011).

[23] A. H. G. Peter, Phys. Rev. D **79**, 103531 (2009).

[24] L. Iorio, J. Cosmol. Astropart. Phys. 05 (2010) 018.

[25] L. Iorio, J. Cosmol. Astropart. Phys. 11 (2010) 046.

[26] M. T. Frandsen and S. Sarkar, Phys. Rev. Lett. **105**, 011301 (2010).

[27] D. T. Cumberbatch, J. A. Guzik, J. Silk, L. S. Watson, and S. M. West, Phys. Rev. D **82**, 103503 (2010).

[28] M. Taoso, F. Iocco, G. Meynet, G. Bertone, and P. Eggenberger, Phys. Rev. D **82**, 083509 (2010).

[29] I. Goldman and S. Nussinov, Phys. Rev. D **40**, 3221 (1989).

[30] G. Bertone and M. Fairbairn, Phys. Rev. D **77**, 043515 (2008).

[31] C. Kouvaris, Phys. Rev. D **77**, 023006 (2008).

[32] C. Kouvaris and P. Tinyakov, Phys. Rev. D **82**, 063531 (2010).

[33] A. de Lavallaz and M. Fairbairn, Phys. Rev. D **81**, 123521 (2010).

[34] D. E. Kaplan, M. A. Luty, and K. M. Zurek, Phys. Rev. D **79**, 115016 (2009).

[35] F. Saudin and P. Ciarcelluti, Astropart. Phys. **32**, 278 (2009).

[36] P. Ciarcelluti and F. Sandin, Phys. Lett. B **695**, 19 (2011).

[37] S.-C. Leung, M.-C. Chu, and L.-M. Lin, Phys. Rev. D **84**, 107301 (2011).

[38] B. Carter, in *Relativistic Fluid Dynamics (Noto, 1987)*, edited by A. Anile and M. Choquet-Bruhat, Lecture Notes in Mathematics Vol. 1385 (Springer-Verlag, Heidelberg, Germany, 1989), pp. 1–64.

[39] G. L. Comer, D. Langlois, and L. M. Lin, Phys. Rev. D **60**, 104025 (1999).

[40] N. Andersson and G. L. Comer, Classical Quantum Gravity **18**, 969 (2001).

[41] N. Andersson, G. L. Comer, and D. Langlois, Phys. Rev. D **66**, 104002 (2002).

[42] R. Prix, J. Novak, and G. L. Comer, Phys. Rev. D **71**, 043005 (2005).

[43] A. Akmal, V. R. Pandharipande, and D. G. Ravenhall, Phys. Rev. C **58**, 1804 (1998).

[44] M. Baldo, I. Bombaci, and G. F. Burgio, Astron. Astrophys. **328**, 274 (1997).

[45] J. B. Hartle, Astrophys. J. **150**, 1005 (1967).

[46] M. Bejger and P. Haensel, Astron. Astrophys. **396**, 917 (2002).

[47] S. Chandrasekhar, Astrophys. J. **140**, 417 (1964).